

# Randomly sampling the chromospheric peak power distribution

J.G. Doyle<sup>1</sup>, G.H.J. van den Oord<sup>2</sup>, and E. O'Shea<sup>1</sup>

<sup>1</sup> Armagh Observatory, College Hill, Armagh BT61 9DG, Northern Ireland (email: jgd@star.arm.ac.uk; eos@star.arm.ac.uk)

<sup>2</sup> Sterrekundig Instituut, P.O. Box 80.000, 3508 TA Utrecht, The Netherlands (G.H.J.vandenOord@fys.ruu.nl)

Received 1 April 1997 / Accepted 16 June 1997

**Abstract.** We have analyzed the UV continuum light curves of 2535 pixels obtained during fifteen separate observations of active regions with the Ultraviolet Spectrometer and Polarimeter (UVSP) on board the solar maximum mission in 1989. Specifically we have looked for periodicities. In the power spectra of 738 light curves (i.e., 29%), evidence was found for periodicities at multiple frequencies. For each power spectrum, containing significant power, we determined the frequency at which the maximum power is found. The distribution  $N(\nu)$ , which describes the number of pixels having maximum power at frequency  $\nu$ , is strongly concentrated in the 2–5 mHz band with a distinct maximum at 3–3.5 mHz. No pixels had their maximum power above 10 mHz and only a few had their maximum power in the 5–10 mHz range. The oscillations in the 2–5 mHz range are probably related to evanescent acoustic waves driven by the photospheric five minute oscillations. In the 2–5 mHz band, the distribution  $N(\nu)$  resembles very much the power spectra as have been observed near the temperature minimum. This suggests that the photospheric power distribution can be interpreted as a probability distribution for finding a given frequency in the UV continuum light curves. In the 2–5 mHz band the spread of the maximum powers and the spread of the count rates, at any frequency, is much larger than above 5 mHz where both are relatively constant. No clear correlation is found between the maximum power and the count rate in a pixel. Furthermore, no evidence is found for emission from the shocks which have recently been invoked to explain the formation of Ca II grains. Whether this is due to temperature effects is unclear. Our general procedure adopted to estimate the confidence level in the power spectrum of a light curve containing photon noise can be equally applied to SUMER and CDS data from SOHO.

**Key words:** methods: data analysis – Sun: chromosphere – Sun: oscillations – Sun: UV radiation

---

## 1. Introduction

With the launch of SOHO new opportunities have become available for studying chromospheric dynamics and, especially, chro-

mospheric oscillations at UV wavelengths. The study of chromospheric oscillations is to a large extent based on optical observations (see e.g. review by Rutten, 1995), while at ultraviolet wavelengths the number of studies is relatively limited. At the end of the seventies several studies of chromospheric oscillations were made based on OSO 8 data (Athay and White, 1979ab, White and Athay, 1979ab, Chipman, 1978, Bruner, 1978, 1981). The OSO 8 data made it possible to study oscillations both in the upper chromosphere (Fe II, Si II, C II) and the transition region (C IV). Although the results of these studies are sometimes conflicting, it could be established that the presence of sound waves is relatively common in the chromosphere, while in the transition region sound waves are not always found. No evidence was found for the existence of a chromospheric cavity as was predicted by Ando and Osaki (1975). An important result of the OSO 8 studies is that the energy flux carried by acoustic waves in the chromosphere is too low to account for coronal heating. For further discussion on chromospheric and coronal heating via acoustic waves, see Narain and Ulmschneider (1996).

In the low chromosphere oscillations with periods of 180–240 s are found (Deubner, 1981) although it is not clear whether these are propagating or evanescent. For example, Lites and Chipman (1979) conclude that in the lower chromosphere 5 minute oscillations are evanescent while waves with frequencies above 5 mHz (200 s) are propagating.

For the upper chromosphere Chipman (1978) found that not all observations show evidence of oscillations but that, when oscillations are present, these have periods near 300 s. Chipman concludes that the associated waves are evanescent. Some of Chipman's results are at variance with those of Athay and White (1979ab) and White and Athay (1979a) who studied a pair of Si II lines. These authors conclude that periods near 300 s are almost always present. The power spectra (line intensities and Doppler shifts) have broad maxima, in the 2.5–9 mHz range, which are superimposed on a flat noise continuum which extends up to 30 mHz and contains most of the power. The waves near 300 s seem to propagate vertically. In the 2.5–9 mHz range delays in the oscillations of the lines, which are formed at different heights, are consistent with upward propagating waves

*Send offprint requests to:* J.G. Doyle

although the phase differences between intensity variations and velocities do not conform to those expected for sound waves.

For the transition region Athay and White (1979b) find that low-amplitude aperiodic fluctuations characterize the data (C IV line) and that only 20% of the datasets show periodic observations in the 3–5 mHz range. These authors argue that the OSO 8 C IV results are indicative of the presence of sound waves in the transition region whose periodicity is sometimes destroyed due to propagation through the chromosphere. Similar conclusions were reached by Bruner (1978) who also found (Bruner, 1981) that the acoustic fluxes in the up- and downward direction almost balance.

OSO 8 had a spatial resolution of  $1 - 2 \times 20 \text{ arcsec}^2$ . An improvement of the spatial resolution was achieved with the launch of the Ultraviolet Spectrometer and Polarimeter (UVSP) on board the Solar Maximum Mission (SMM). Surprisingly the number of oscillation studies with UVSP is relatively limited. A number of studies focussed on transition region oscillations above sunspots (Gurman et al., 1982, Henze et al., 1984, Thomas et al., 1987), using mainly the C IV line. Bruner and Poletto (1984) conclude from N V (1238Å) observations that there is a net upwardly directed acoustic flux (contrary to Bruner, 1978).

From a rather arbitrary sample of (continuum) light curves of active regions Drake et al. (1989) conclude that periods in the range 4–5 min. (3.3–4.2 mHz) are ubiquitously present while occasionally periods down to 3 min. (5.6 mHz) are seen.

In this paper we discuss the UVSP observations of a number of active regions in order to extend the study by Drake et al. (1989). Although UVSP does not have the diagnostic capabilities of e.g. SUMER and CDS on board SOHO, it is interesting to see which periodicities are present in the UV.

Any analysis of oscillatory phenomenon is necessarily based on Fourier techniques. For observations based on individual photon counts the problem of noise is especially noteworthy. It is important to establish the statistical significance for any feature in a power spectrum resulting from a Fourier transform. Fortunately, this problem has received considerable attention in the X-ray community working on QPO phenomenon. Based on that work we discuss in this paper several effects of noise in power spectra and how the noise levels can be determined. The described techniques are equally applicable to SUMER and CDS data.

The outline of the paper is as follows. In Sect. 2 we describe the observations and the spectral properties of the UVSP band-pass. In Sect. 3 the method of analysis is described which is applied to the UVSP data in Sect. 4. Our conclusions are presented in Sect. 5.

## 2. Observational data

The observations described here were taken during June to August 1989 with the UVSP instrument on board the SMM satellite. During this time a number of different active regions were observed. The particular active regions which are of interest to us in this work, their UVSP experiment numbers and the time and date at which the rasters were taken, are given in Table 1.

**Table 1.** A summary of the UVSP datasets used in this analysis.

NOAA AR	Exp. No.	Date / Time
5515	89750	1 Jun '89 02:53
5555	91232	23 Jul '89 20:13
5589	92661	18 Jul '89 07:55
5589	92704	19 Jul '89 07:02
5589	92712	19 Jul '89 13:12
5598	92746	20 Jul '89 04:36
5598	92750	20 Jul '89 07:41
5598	92752	20 Jul '89 09:13
5598	92789	21 Jul '89 08:20
5597	92856	22 Jul '89 21:18
5606	92917	24 Jul '89 08:43
5606	92921	24 Jul '89 11:48
5597	92939	24 Jul '89 19:30
5608	93113	28 Jul '89 20:30
5643	94400	18 Aug '89 02:46

The UVSP instrument (Woodgate et al., 1980) consisted of a Gregorian telescope, a polarimeter consisting of two retarders and a linear polarizer, an Ebert-Fastie spectrograph and five photomultiplier detectors (four used in second order, 1170–1780Å and one in first order, 1780–3600Å). Unfortunately from July 1985 onwards the wavelength drive of UVSP was inoperable and all 2nd order UVSP observations were restricted to a wavelength in the  $\sim 1373.5\text{--}1375.8\text{Å}$  range (Henze, 1993). The observations discussed in this paper were obtained using a slit with an exit width of  $2.3\text{Å}$ . The above spectral window does not contain strong ultraviolet lines. According to the quiet sun model of Vernazza et al. (1981), the continuum in this region is due to Si I which is found in the lower chromosphere at a height above the photosphere of 600–800 kilometers ( $T \approx 5000\text{ K}$ ; we return to this point later). Unfortunately, there was no simultaneous ground-based coverage, although for some of the days involved, either magnetograms or He I 10830Å images are available for times within a few hours of the UVSP data. An example of this is given in Fig. 1 where a Kitt Peak magnetogram (taken on 19 July '89 17:54 UT) is over-plotted with the UVSP data which started at 13:12 UT July 19.

For all the UVSP experiments analyzed here, the field of view used was  $70 \times 70 \text{ arcsec}^2$ , rastered in steps of 5 arcsec. The individual pixel size was  $10 \times 10 \text{ arcsec}^2$  which means an overlap of 5 arcsec from one pixel to the next in the raster. The time taken for a typical raster of  $13 \times 13$  pixels was  $\sim 22$  seconds, with each pixel having an integration time of 0.112 seconds. Including overheads, the typical gate time was 0.128 sec. A typical experiment involved repeated rastering of the region of interest, which implied for a 129 point raster a total duration of  $\sim 45$  minutes. Normally, the last few rasters could not be used.

This work is a followup to an earlier analysis by Drake et al. (1989) who studied several datasets taken in July 1988. In that work, Drake et al. looked at three types of variability; flares, bursts and oscillations. It is the oscillation-type that is the main subject of the present work. This earlier work noted the presence

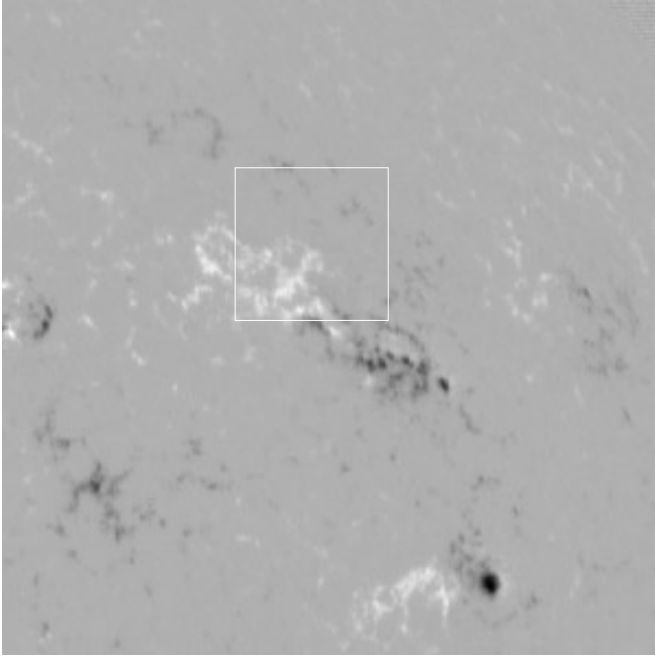


**Fig. 1.** A  $300 \times 300 \text{ arcsec}^2$  magnetogram obtained on 19 July 1989 17:54 with an  $70 \times 70 \text{ arcsec}^2$  outline of the position of the UVSP dataset series 92712 obtained  $\sim 4.5$  hrs. earlier.

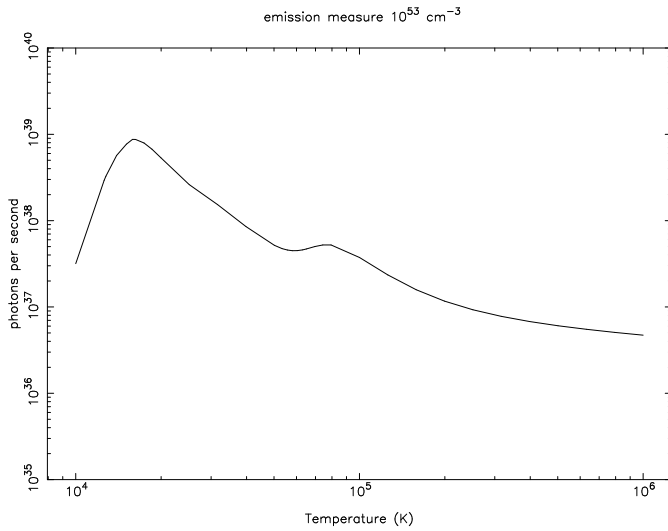


**Fig. 2.** Photon flux (at the source) in the UVSP bandpass ( $1373.5\text{\AA}$ – $1373.8\text{\AA}$ ) for an emission measure of  $10^{53} \text{ cm}^{-3}$ .

of oscillations in the 3–5 min. range and concluded that these were of solar origin as opposed to artifacts due to instruments drifts. There are essential two main reasons why these can not be instrumental; (i) the entrance slit used was  $10 \times 10 \text{ arcsec}^2$ , thus only pointing drifts approaching  $10 \text{ arcsec}$  could produce such oscillations and these were very rare in the pointing, (ii) in the  $13 \times 13$  pixel raster not all the pixels showed this type of periodicity, normally a few adjacent pixels would show an oscillation while the next few pixels would have no periodic variability.

The different datasets given in Table 1 and the resulting 169 individual light curves (from the  $13 \times 13$  pixels) in each dataset were reduced by the Fourier analysis technique as outlined in Sect. 3.

In order to interpret the observed emission it is also useful to consider the emission expected from an optically thin plasma in collisional equilibrium. Using the spectral code SPEX (Kaastra et al., 1996) we determined the emissivity in the UVSP bandpass ( $1373.5\text{\AA}$ – $1375.8\text{\AA}$ ) under the assumption of solar photospheric abundances (Anders and Grevesse, 1989). The resulting emissivity (photons/sec.) as a function of temperature is shown in Fig. 2 for an assumed emission measure of  $10^{53} \text{ cm}^{-3}$ . In order to get the observed flux we divide by  $4\pi d^2$  with  $d$  the distance of the source. The observed emission consists only of continuum emission (the nearest line is that from OV at  $1371.3\text{\AA}$ ). At temperatures below  $10^5 \text{ K}$  the main contribution to the UVSP continuum is by two-photon emission. Above  $10^6 \text{ K}$  free-free emission starts to dominate. Note that the vertical axis has a logarithmic scale. The emissivity has a strong peak at a temperature of  $15850 \text{ K}$  and the main contribution, say  $>0.1 \times$  maximum, is in the temperature range  $11000$ – $39000 \text{ K}$ . In the optically thin interpretation the photon flux scales with the density squared times the emissivity. The shape of the emissivity curves indicates that at temperatures lower than  $15850 \text{ K}$  the photon flux is more sensitive to changes in the temperature while at higher temperature it is more sensitive to density variations.

### 3. The fourier transform

In this section we discuss the effects of data sampling on the Fourier transform. The Fourier transform  $a(\nu)$  of a continuous function  $x(t)$  is defined by

$$a(\nu) = \int_{-\infty}^{\infty} x(t)e^{2\pi i\nu t} dt, \quad (1)$$

and its inverse by

$$x(t) = \int_{-\infty}^{\infty} a(\nu)e^{-2\pi i\nu t} d\nu. \quad (2)$$

When the function  $x(t)$  consists of  $N$  discrete measurements  $x_k$  ( $k = 0, \dots, N-1$ ), which constitute an equidistant time series of length  $T$ , then the discrete Fourier transform results in  $N$  values  $a_j$  ( $j = -N/2, \dots, N/2 - 1$ ) for the Fourier components

$$a_j = \sum_{k=0}^{N-1} x_k e^{2\pi i j k / N}. \quad (3)$$

The inverse discrete transform is given by

$$x_k = \frac{1}{N} \sum_{j=-N/2}^{N/2-1} a_j e^{-2\pi i j k / N}. \quad (4)$$

In these expressions  $x_k = x(t_k)$  with  $t_k \equiv kT/N$  so that the time steps are given by  $\delta t = T/N$ . The coefficients  $a_j$  are related

to the frequencies  $\nu_j = j/T$  so that the resolution in frequency is given by  $\delta\nu = 1/T$ . The highest frequency, corresponding to the Nyquist frequency, is given by  $\nu_{N/2} = N/(2T)$ . Note that  $a_0 = \sum_k x_k$  corresponds in our case to the total number of photons  $N_{\text{ph}}$  detected during time  $T$ . We define the power spectrum as

$$P_j = \frac{2}{N_{\text{ph}}} |a_j|^2 = \frac{2}{a_0} |a_j|^2 \quad j = 0, \dots, N/2. \quad (5)$$

The relation between the continuous and the discrete Fourier transform for the datasets considered in this paper can be derived as follows. Each dataset consists of  $N$  measurements of the photon counts in a specific pixel. Each individual measurement consists of integrating the photon counts over a short time interval of length  $\tau$ . The total length of the time series is  $T$ . Let  $x(t)$  be the number of photons arriving from the source at time  $t$ . Because of the finite integration time  $\tau$  the actual photon flux which is sampled corresponds to a function  $y(t) = x(t) * b(t)$  with  $*$  indicating a (Fourier) convolution and with  $b(t)$  the binning function

$$b(t) = \begin{cases} 1/\tau & -\tau/2 < t < \tau/2, \\ 0 & \text{otherwise.} \end{cases} \quad (6)$$

The convolution of  $x(t)$  and  $b(t)$  corresponds to averaging the actual photon counts over a bin of width  $\tau$  around time  $t$  so that  $y(t)$  is given by

$$y(t) = x(t) * b(t) = \int_{-\infty}^{\infty} x(t-t')b(t')dt' = \frac{1}{\tau} \int_{t-\tau/2}^{t+\tau/2} x(u)du.$$

The discrete sampling of the data amounts to multiplying the function  $y(t)$  with a window function  $w(t)$  and with a sampling function  $s(t)$ . The window function is given by

$$w(t) = \begin{cases} 1 & 0 \leq t \leq T, \\ 0 & \text{otherwise} \end{cases} \quad (7)$$

and the sampling function by

$$s(t) = \sum_{k=-\infty}^{\infty} \delta(t - kT/N). \quad (8)$$

The sampling function indicates that function  $y(t)$  is discretely sampled at times  $t_k = kT/N$  while the window function accounts for the finite duration of the time series. Let  $y_m$  indicate a measured time series. From the discussion above it follows that  $y_m = y(t)w(t)s(t)$ . Let  $\mathcal{F}$  denote the Fourier transform and let  $Y \equiv \mathcal{F}(y)$ ,  $S \equiv \mathcal{F}(s)$  and  $W \equiv \mathcal{F}(w)$ . Then the Fourier transform of the measured time series  $y_m$  is given by

$$\mathcal{F}(y_m) \equiv a(\nu) = Y(\nu) * W(\nu) * S(\nu), \quad (9)$$

with

$$W(\nu) = \frac{i}{2\pi\nu} (1 - e^{2\pi i\nu T}), \quad (10)$$

$$S(\nu) = \frac{N}{T} \sum_{\ell=-\infty}^{\infty} \delta(\nu - \ell \frac{N}{T}). \quad (11)$$

From Eq. (9) we find that

$$\mathcal{F}(y_m) = \sum_{k=0}^{N-1} y(t_k) e^{2\pi i\nu kT/N}. \quad (12)$$

The relation of the continuous Fourier transform and the discrete transform is established by taking  $\nu_j = j/T$  so that

$$a_j = a(\nu_j) = \sum_{k=0}^{N-1} y(t_k) e^{2\pi ijk/N}. \quad (13)$$

The components of the power spectrum are then given by

$$P_j = \frac{2}{a_0} \times \left\{ \left( \sum_{k=0}^{N-1} y(t_k) \cos\left(\frac{2\pi jk}{N}\right) \right)^2 + \left( \sum_{k=0}^{N-1} y(t_k) \sin\left(\frac{2\pi jk}{N}\right) \right)^2 \right\} \quad (14)$$

By studying the power spectrum of the observed counts we obtain information about the function  $y(t)$ . Because  $y(t) = x(t) * b(t)$  we have that  $Y(\nu) = X(\nu)B(\nu)$  with  $X(\nu) = \mathcal{F}(x)$  and

$$B(\nu) = \frac{\sin(\pi\nu\tau)}{\pi\nu\tau}. \quad (15)$$

For the observations described in this paper  $N = 122$ ,  $\tau = 0.128$  s,  $\delta t = 21.7$  s and  $T = (N-1)\delta t = 2626$  s  $\approx 44$  minutes. A sample of 122 data points results in a power spectrum at 62 discrete frequencies (one at zero frequency). The highest frequency, the Nyquist frequency, corresponds to  $\nu_{N/2} = 122/(2T) = 23.2$  mHz or a period of  $P = 43$  seconds. Due to the discrete sampling any period in the signal shorter than 43 seconds will be aliased. In general the process of measuring the data points will automatically result in a suppression of high frequencies so that aliasing is not a too serious problem. However in our case  $\tau$  is only 0.128 seconds so that aliasing will not be suppressed due to the finite time a measurement takes. This can also be seen in Eq. (15). At the Nyquist frequency  $\pi\nu_{N/2}\tau \sim 9 \cdot 10^{-3}$  so that  $B(\nu) \approx 1$  over the whole frequency range considered and hence no suppression of high frequencies occurs. So care has to be exercised for the possibility of aliasing.

A second effect which occurs is caused by the data windowing. Function  $w(t)$  is a box car function with length  $T$ . The transform of the signal is convolved with  $W(\nu)$  which has a central peak of width  $\delta\nu = 1/T$  and side lobes. The effect of windowing is that the power at a given frequency is distributed over neighbouring frequency bins.

A third effect which occurs is due to the use of the discrete Fourier transform. When looking for a periodic signature with frequency  $\nu$ , the associated power is only recovered when  $\nu$  corresponds exactly with one of the frequencies at which the power spectrum is evaluated. When  $\nu$  is exactly in-between two frequency bins the power is distributed over the neighbouring frequency bins and even some bins further away. So the spread of power over adjacent bins is caused by two effects: 1) the finite length of the time series which results in windowing; 2) the

use of the discrete Fourier transform. The effect of windowing can be suppressed by using a window function for the time series which differs from the box car (e.g. Welch, Hanning, Parzen etc.). However, we decided not to use any of the above windowing functions, as such a function broadens the secular variations due to a slow increase/decrease in the counts and therefore affects the determination of the variations we seek to analyse.

The time series can be characterized as follows. The average number of photon counts per 0.128 seconds amounts to a few hundred counts,  $\sim 300 - 400$  in most datasets although, as we will see later, some parts of a dataset can have counts in the 1000–1500 range while other parts are in the 50–100 range. In each dataset, there are secular variations due to a slow decrease or a slow increase of the counts. This occurs on time scales in the range  $0.5T - T$ . Superimposed on these slow variations are faster variations. Simply looking at the time series suggests already that some variations are (quasi-)periodic. The amplitudes of the variations are larger than expected from pure Poisson statistics (e.g.  $300 \pm 17$  or  $400 \pm 20$ ). Because of the high average counting level and the presence of secular variations it can be anticipated that there will be significant power at low frequencies, say  $\nu = 0, 1/T, 2/T$ . This power can be reduced by subtracting some ‘average’ from the observed counts, e.g., a first-order polynomial fit. However, there is little to be gained by this procedure.

A description of the statistical properties of the power spectrum can be found in Jenkins and Watts (1968), Leahy et al. (1983), and is comprehensively summarized in van der Klis (1989). The normalization of the power spectrum (Eq. (5)) is chosen in such a way that if the noise in the data is (only) Poissonian, then the distribution  $P_{j,\text{noise}}$  is given by the  $\chi^2$  distribution with two degrees of freedom (dof). The probability that  $P_{j,\text{noise}}$  exceeds a threshold power level  $P_{\text{threshold}}$  is

$$\text{Prob}(P_{j,\text{noise}} > P_{\text{threshold}}) = Q(P_{\text{threshold}}|2),$$

with  $Q$  the integral probability of the  $\chi^2$  distribution

$$Q(\chi^2|v) = \left(2^{v/2}\Gamma\left(\frac{v}{2}\right)\right)^{-1} \int_{\chi^2}^{\infty} t^{v/2-1} e^{-t/2} dt. \quad (16)$$

For two dof the standard deviation of the noise powers is equal to their mean value  $\sigma_{P_j} = \bar{P}_j = 2$ . This implies that in the power spectrum the magnitude of the noise component is not well defined. There exist basically two methods to decrease the noise in the power spectrum. One method is to rebin the power spectrum by averaging  $W$  consecutive frequency bins at the expense of a reduced frequency resolution. The other method, which can be used in combination with the previous, is to divide the data into  $M$  segments of equal length. For each of the data segments the power spectrum is determined and the resulting power spectra are then averaged. The resulting power distribution of the noise corresponds then to a  $\chi^2$ -distribution with  $2MW$  dof which is scaled with a factor  $1/MW$ . In this case we have that  $\text{Prob}(P_{j,\text{noise}} > P_{\text{threshold}}) = Q(MWP_{\text{threshold}}|2MW)$ . The mean of the distribution is still equal to 2 but the standard

deviation has been reduced to  $2/\sqrt{MW}$ . We note that the noise in the power spectrum can, effectively, only be reduced at the expense of frequency resolution. Increasing the observing time  $T$  will not change the mean and the standard deviation of the noise distribution but, in the end, longer observing times, in combination with segmenting and/or rebinning, do permit reduction of the standard deviation of the noise while achieving an improved frequency resolution.

Suppose that we have a power spectrum at  $N$  frequencies and want to establish which powers have a low probability of being caused by noise. The power at each of the frequencies can be considered as an independent trial. Define  $(1 - \epsilon)$  as the probability that a power  $P_j$  exceeds detection level  $P_{\text{det}}$  and is not caused by noise. For  $N$  independent powers this probability is  $(1 - \epsilon)^{1/N}$  so that the chance to exceed  $P_{\text{det}}$  and to be caused by noise is  $1 - (1 - \epsilon)^{1/N} \approx \epsilon/N$  for  $\epsilon \ll 1$ . From this it follows that the detection level is given by

$$\epsilon/N = Q(MWP_{\text{det}}|2MW). \quad (17)$$

In this paper we use a confidence level of 99.9% ( $\epsilon = 10^{-3}$ ) to determine  $P_{\text{det}}$ . For  $M = W = 1$ , the detection level is given by  $P_{\text{det}} = 2 \ln(N/\epsilon)$ . For  $MW > 1$ , Eq. (17) results in an implicit relation for  $P_{\text{det}}$ .

#### 4. Results

In Figs. 3–5 we show surface plots of the average count rate per pixel, the resulting peak power at the most significant frequency and the most significant frequency above 1.5 mHz in the light curve of a pixel, for all datasets, as derived from time-series analyses without frequency binning (i.e.,  $W=1$ ). Our definition of significant power is the 99.9% confidence level. As can be seen not all pixels within a particular dataset show evidence of an oscillation. However, in some instances, although not in all datasets, individual pixels which do not show a clear wave-like behaviour, if added together, can sometimes show a periodicity in the 3–4 mHz range at the 99.9% confidence level. In most cases, those regions showing a clear oscillation are confined in size. Sometimes, it can be a single pixel, thus less than  $10 \times 10 \text{ arcsec}^2$ . In other instances, the spatial size can approach a few pixels.

In Fig. 6, we show the light-curve plus the resulting power spectrum for a group of 11 pixels (showing excess signal) from the central region of dataset 92712 (note that in this figure, two adjacent frequency bins were averaged, i.e.,  $W=2$ ). As can be clearly seen, excess signal at 3.0 and 3.7 mHz is present corresponding to periods of 330 sec and 270 sec respectively. These periods are similar to those derived by Drake et al. (1989). In dataset 92712, there is no evidence of flare-like activity, although in some datasets the observed periodicities are flare-like. As an example, we show in Fig. 7 the light-curve and power spectrum for dataset 92921. As can be clearly seen in the light-curve, there is a series of short duration bursts which are of a flare-like appearance. The time lag between these events ranges from 6 to 10 mins. This can also be seen from the power spec-

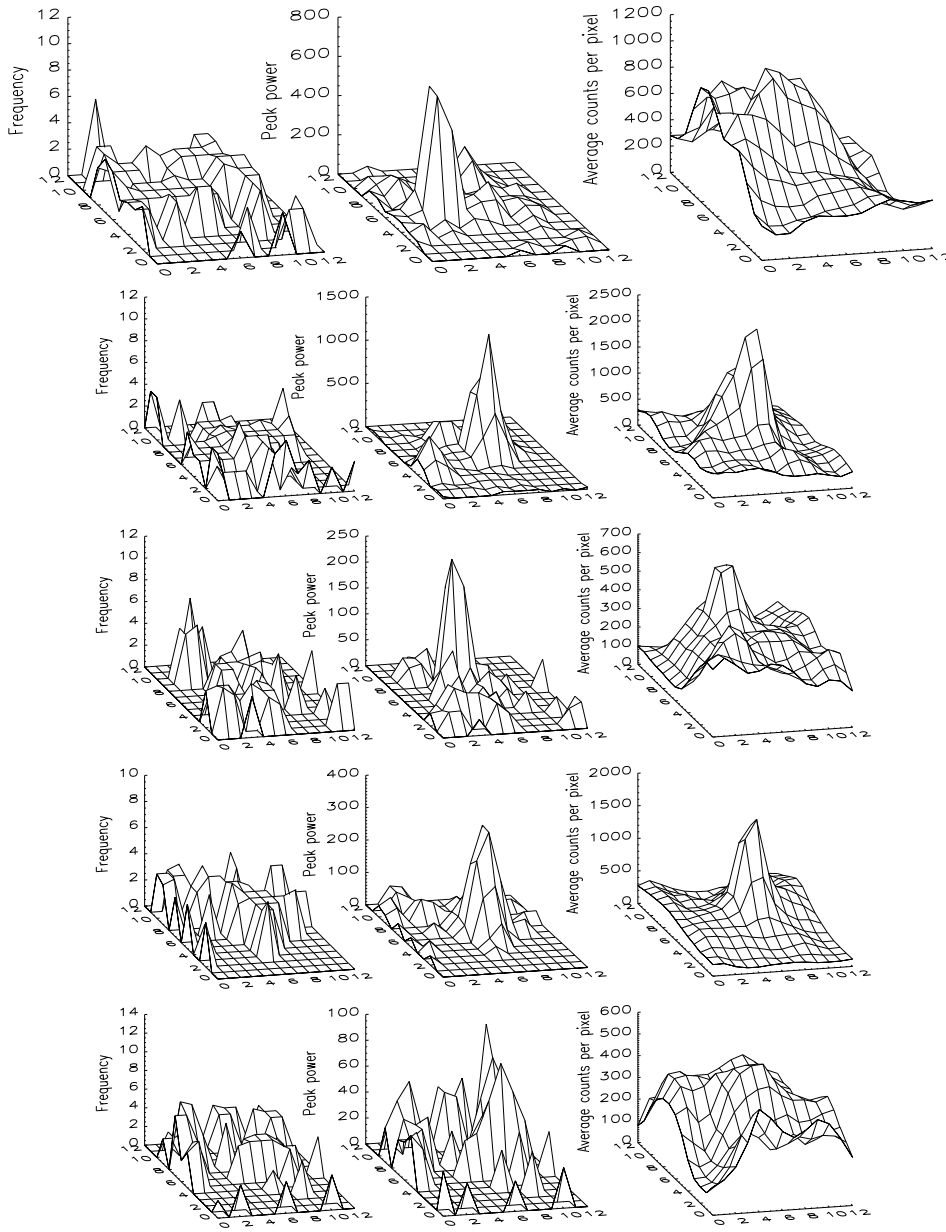


**Fig. 3.** Surface plots of the peak frequency above the 99.9% confidence level, the peak power and the count rate for datasets 89750, 91232, 92661, 92704 and 92712 (from top to bottom). **89750:**... the brighter pixels, e.g. those approaching 1000 cts per integration time, have frequencies close to 2 mHz.. by adding together pixels which do not individually show significant power we can derive a significant signal at 3.3 mHz, this region corresponds to pixels adjacent to pixels showing an excess signal, on-the-other-hand, taking a large group of pixels far removed from those showing excess signal results in a null detection and to a reduced count-rate compared to the remainder of the dataset; **91232:**... as in 89750 the brighter pixels correspond to lower frequency... again by adding individual pixels which do not reach the 99.9% confidence level we can obtain significant power at 4 mHz, although there are regions where no excess signal can be detected.. the count-rate in these regions are similar to those where an excess signal is present; **92661:**... nice group of pixels showing significant power at 3.0/3.3 mHz, although there are many pixels which do not show significant power; **92704:**... similar to 92661; **92712:**... excellent group of pixels showing 3.0/3.7 mHz signal.

trum which shows peaks corresponding to these periods, plus a range of shorter periods in the range 2–4 mins.

In many datasets, as can be seen in Fig. 6, the  $\sim 5$  min. period has at least 9 cycles. However, this is not the case for the longer periods perhaps because our datasets are only of  $\sim 44$  min duration, thus a wave with a period approaching 10 mins. can have at most 4 cycles.

Our data comprise the light curves of  $15 \times 13^2 = 2535$  pixels. In the power spectra of 738 light curves, (29%) statistically significant power peaks were found. In most of the cases significant power was found at multiple frequencies. Above  $\sim 6$ –10 mHz the power, in general, varies around 2, the value expected from a (Poissonian) noise distribution. For each of the light curves containing significant power, we determined the frequency above  $\sim 2$  mHz at which the maximum power (peak power) was found. The distribution of the number of pixels with a peak power at a given frequency is shown in Fig. 8. Because three datasets were

analyzed with a slightly different frequency grid we show these separately in Figs. 8b–8d while Fig. 8a is based on the twelve other datasets. Fig. 8a shows that for the majority of the datasets the most dominant powers are found in the 2–5 mHz range with a distinct maximum around 3 mHz. Only a few pixels have their peak power in the 6–10 mHz range. For most of the datasets the number of pixels with a peak power around 2 mHz is small. However, the data set shown in Fig. 8c contains a large number of pixels with peak powers at 2 mHz (8.3 min.). These pixels are often associated with flare-like brightnings and have high count rates.

For all datasets, we show in Fig. 9a the distribution of the peak powers as a function of frequency and in Fig. 9b the average count rate as a function of frequency. Note that these figures show a ‘vertical band’ structure at certain frequencies because of the different frequency grid used for three datasets. Because the power is normalized according to Eq. (5), the 99.9% confidence

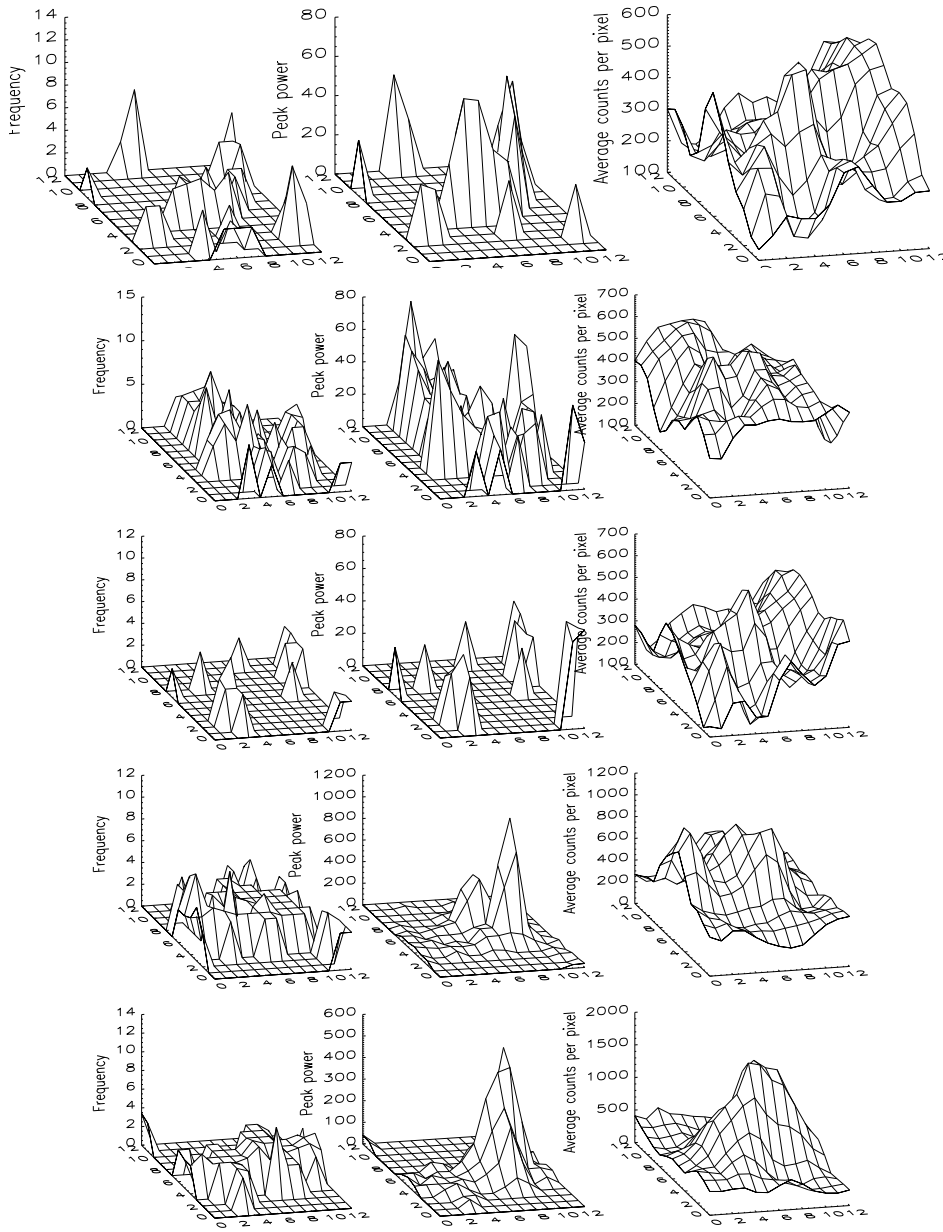


**Fig. 4.** Surface plots of the peak frequency above the 99.9% confidence level, the peak power the count rate for datasets 92746, 92750, 92752, 92789 and 92856 (from top to bottom). **92746:**... only a few pixels show a periodicity; **92750:**... some very good 3.0 mHz pixels, again as in 91232 some individual pixels not reaching the 99.9% confidence level if added can become significant around 4 mHz; **92752:**... only a few pixels show a periodicity... taking a large group of pixels far removed from those showing excess signal results in a null detection; **92789:**... several high count-rate pixels show significant power at 3 mHz, on-the-other-hand there are several pixels with a very low count-rate that do not show evidence for periodicity even if added together; **92856:**... only a few pixels show a periodicity.

level corresponds to about 23. This explains the minimum power level in the figure. Also, the power at which a data point is found is a direct measure of its significance level. Because we put our detection limit at the 99.9% confidence level, the powers shown in Fig. 9a are extremely significant. The strongest powers are found in the 2–5 mHz range although the magnitude of the power strongly varies. Between 6–10 mHz the distribution of the peak powers, in terms of their significance, is relatively flat.

The highest count rates are found for frequencies around 2 mHz and are associated with flare-like brightenings (Fig. 9b). Most pixels with significant power in the range 2–10 mHz have average count rates of 200–600 counts/second. However, between 2 and 5 mHz, the pixels show a larger spread of the count rate than above 5 mHz. Fig. 9c shows that there is a weak correlation between the count rate and the peak power in the sense that as the count rate increases the spread in the powers increases. This could, however, be a selection effect because low count

rates are necessarily related to a relatively larger Poisson noise and lower (unnormalized) powers. On the other hand, Figs. 3–5 demonstrate that high count rates do not always result in the detection of significant peaks in the power spectrum. From this we conclude that there is no clear correlation between the presence of a significant period and the count rate.

## 5. Discussion and conclusions

We have analyzed the light curves of the individual pixels of 15 UVSP data sets and specifically looked for evidence of chromospheric oscillations. Only in a limited number of pixels (29%), did we find evidence of periodicities. For those pixels, which show periodicities, the maximum power is predominantly found between 2 and 5 mHz with a distinct maximum around 3–3.5 mHz. The highest count rates are found for frequencies of 2 mHz and are associated with flare-like brightenings.

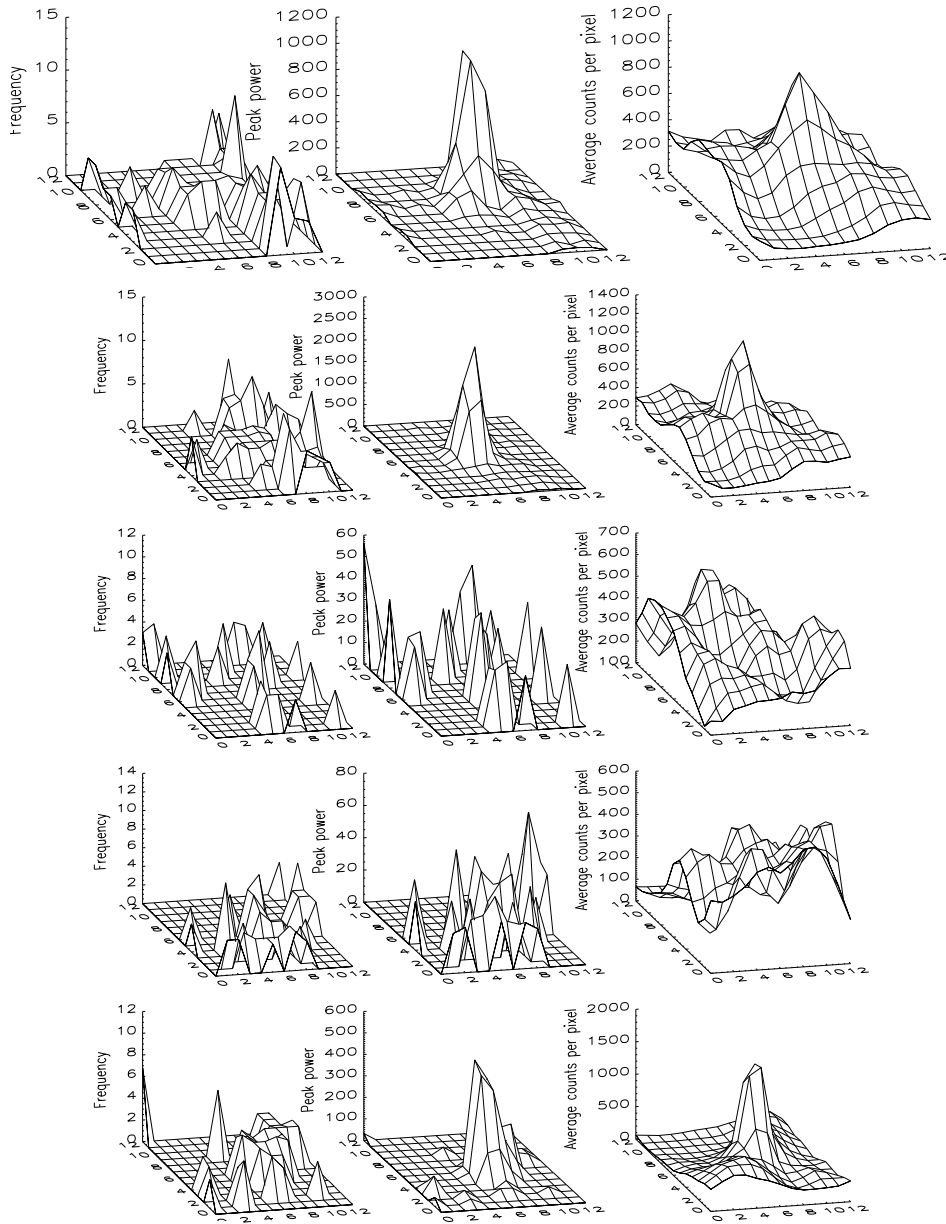


**Fig. 5.** Surface plots of the peak frequency above the 99.9% confidence level, the peak power and the count rate for datasets 92917, 92921, 92939, 93113 and 94400 (from top to bottom). **92917:**... as in 92789, several pixels with a very low count-rate even if added together do not show evidence for periodicity; **92921:**... nice group of bright pixels showing significant power at 2 mHz; **92939:**... only a few pixels show a periodicity; **93113:**... only a few pixels show a periodicity, also as in 92789, several low count-rate pixels even if added together do not show evidence of a periodicity; **94400:**... only a few pixels show a periodicity.

The distribution of peak powers shown in Fig. 8a has a strong resemblance with the power distribution of the photospheric five minute oscillations as derived from Doppler shifts of C I and Fe I lines (see e.g. Fig. 1 in Rutten, 1995). This is a bit surprising because there is no *a priori* reason to expect that when at different spatial locations the peak power in the UVSP bandpass is measured, it would correspond to such a distribution. Alternatively one can argue that the photospheric five minute oscillations are not a stationary phenomenon but consist of distinct wave packets of finite duration. The power spectra of C I and Fe I lines can then be interpreted as the probability distributions for finding power at a given frequency. The measurements described in this paper should then be interpreted as a random sampling of this probability distribution. The distribution shown in Fig. 8a is clearly not representative of a distribution one would expect for the chromospheric three minute oscillations as observed in

Ca II. Such a distribution is broad (2–10 mHz) and centered around 5.5 mHz.

A key question is where in the chromosphere the continuum in the UVSP bandpass has its origin. In the Vernazza et al. (1981) models it is formed in the lower chromosphere at  $T \approx 5000$  K. From a black body with this temperature, and an area of  $10 \times 10$  arcsec<sup>2</sup>, the number of photons is  $5 \cdot 10^{31}$  photons/s/pixel in the UVSP bandpass. If, on the contrary, the emission is optically thin we can use the Vernazza et al. chromospheric models to calculate the emission measure of the plasma in the temperature range 11,000–39,000 K. Multiplying this number with the area of an UVSP pixel gives for a pixel an emission measure of  $5 \cdot 10^{45}$  cm<sup>-3</sup>. From the emissivity curve (Fig. 2) we estimate the number of photons in the optically thin interpretation to be  $\sim 10^{31}$  photons/s/pixel which is a factor five less than the number of photons in the optically thick interpretation. We checked that the contribution by any overlying coronal

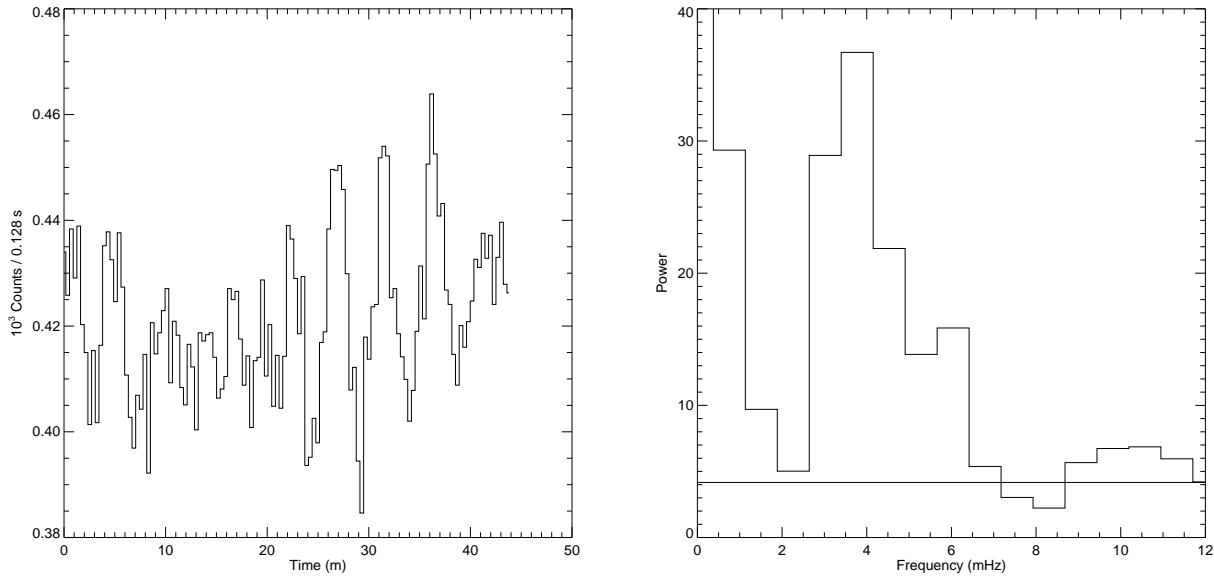


**Fig. 6.** Light-curve and power spectrum for the average of the 11 pixels corresponding to the bright region within image 92712. Note that we have applied a binning by a factor of two in frequency.

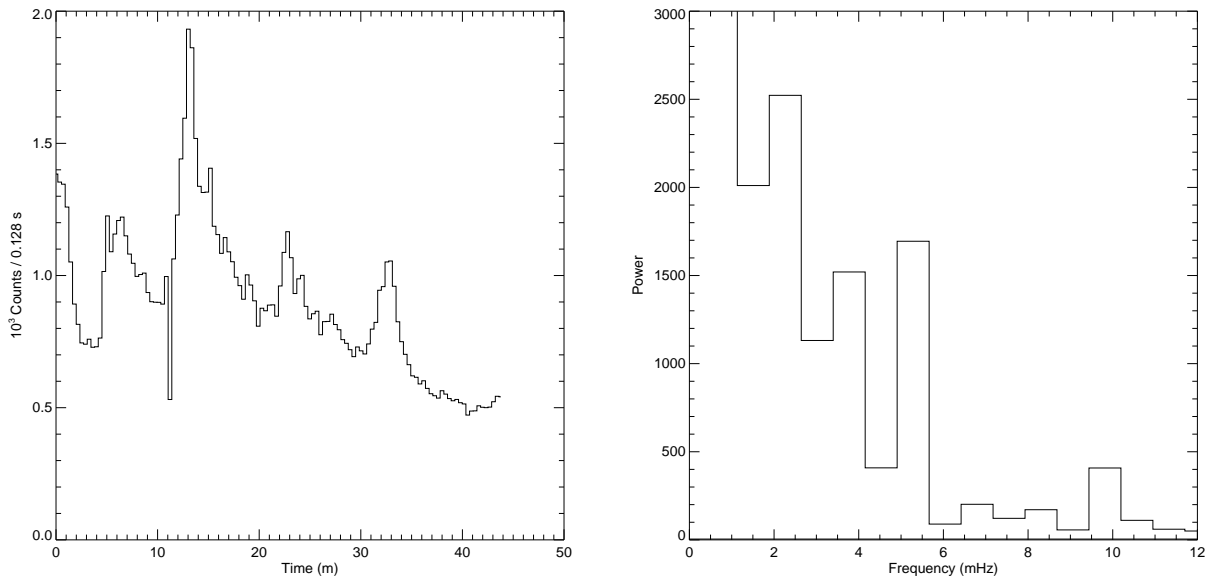


**Fig. 7.** Light-curve and power spectrum for the average of the 8 pixels corresponding to the bright region within image 92921. Note that we have applied a binning by a factor of two in frequency.

plasma is negligible. This implies that the bulk of the observed emission is optically thick emission from the lower chromosphere with a small ( $\sim 20\%$ ) optically thin contribution from the overlying chromospheric layers. We note however that if the true chromospheric densities would be a factor three higher than in the Vernazza et al models, then the optically thin component in the temperature range 11,000 - 39,000 K would dominate the observed emission.

Recently Carlsson and Stein presented in a number of papers (1992, 1994, 1995, 1997) a very dynamical picture of the chromosphere. These authors demonstrated that the formation

of Ca II H&K grains is related to the presence of shocks. Because in a shock the temperature and the density increase, it is interesting to see whether the oscillations observed in the UVSP bandpass are related to such shocks. In Carlsson and Stein (1994) it is shown that the chromosphere has a multi-temperature structure with locally very high (shocks) and very low temperatures. The mean temperature is however relatively low (4000–5000 K). The high-temperature spikes in the shocks raise the observed brightness temperature above the true mean temperature. In Fig. 5 of Carlsson and Stein (1995, or Fig. 11 of Rutten, 1995) these authors do not show the shock tem-

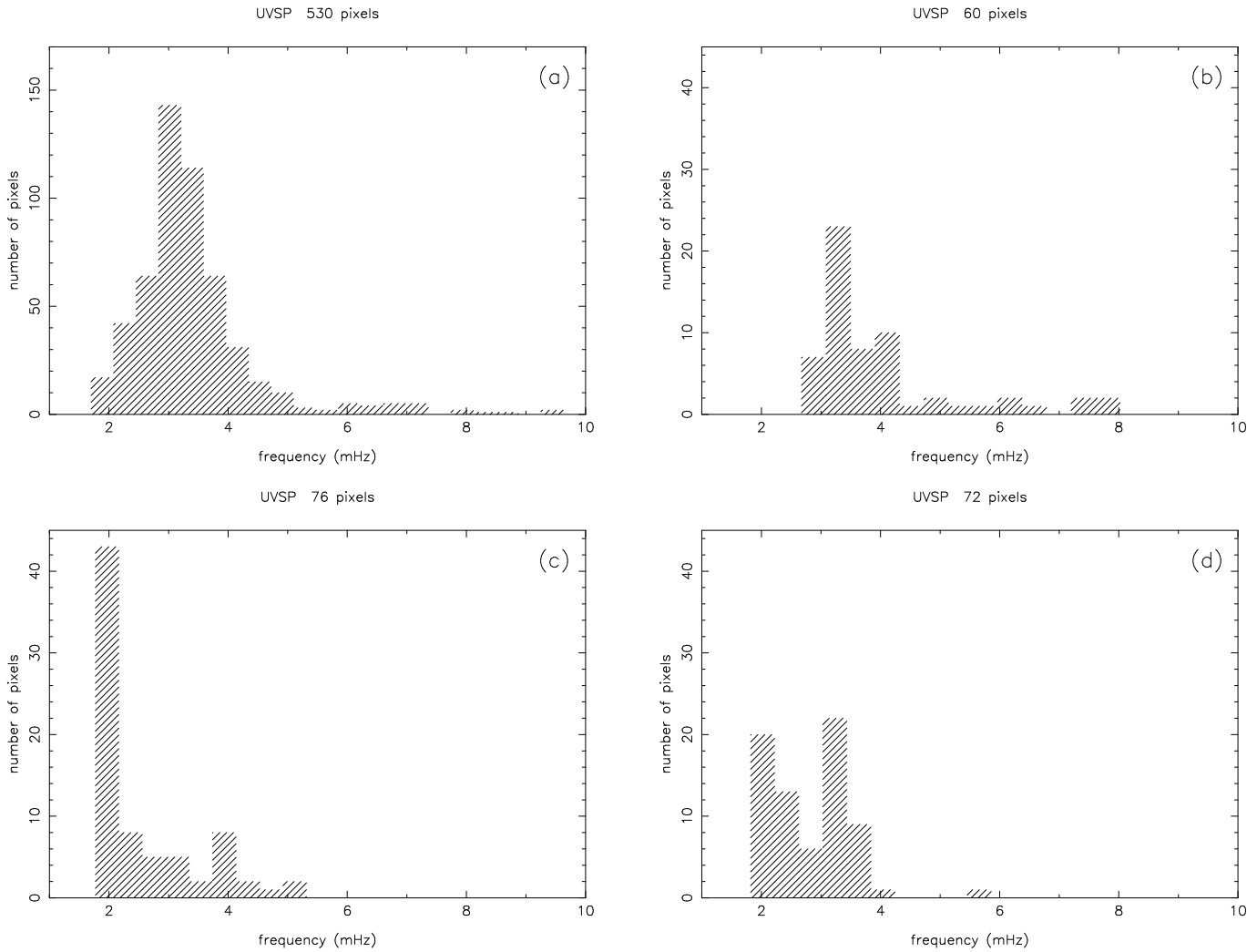


**Fig. 8a–d.** Histograms showing the number of pixels as a function of frequency. For each pixel the most significant power is determined and at that frequency the pixel is included in the distribution. Most datasets were analyzed with the same frequency grid (distribution shown in **a**) but for three datasets a slightly different frequency grid was used (shown in **b** is dataset 92750, **c** is dataset 91232 and **d** is dataset 89750). Above 10 mHz no significant power peaks were found.

temperatures above  $10^4$  K but higher up in the chromosphere the shocks will further steepen and reach temperatures at which the emissivity curve for the UVSP continuum region, shown in Fig. 2, has its maximum. In their 1997 paper Carlsson and Stein demonstrate that the Ca II grains are associated with either isolated or merging shocks. Apart of the relevance of this work for grain formation, the simulations by Carlsson and Stein also provide information about wave propagation in the chromosphere. Therefore we discuss in the following various aspects of these simulations. Carlsson and Stein start with an atmosphere in radiative equilibrium which is perturbed by a piston at the base. The velocity profile of the piston is chosen so that (slightly higher up in the atmosphere) the observed velocity profile of an Fe I line is mimicked. Most of the photospheric (piston) power is in the frequency range 2–6 mHz. Carlsson and Stein distinguish three frequency ranges: 0–4.7 mHz (low:L), 4.7–7.1 mHz (medium:M) and above 7.1 mHz (high:H). Simu-

lations with the piston only driven in the L range do not produce shocks and grains. The reason is that these frequencies are below the acoustic cut-off frequency so that the waves are evanescent. Simulations with the piston only driven in the M or H frequency band do produce shocks and grains, because the waves can propagate and steepen, but not in agreement with the observed grain patterns. A good correspondence with the observed patterns is found when the piston is driven over the full frequency range. In that case the following picture arises: only waves with frequencies  $\geq 4.7$  mHz can propagate and steepen into shock. The largest photospheric power at these frequencies is found close to the cut-off frequency so that most shock associated grains have this frequency. It is the combination of a broad spectrum of waves, the acoustic cut-off frequency and the photospheric power distribution which results in the specific time behaviour of the grains and shocks. Our results in Fig. 8a do not show a maximum for the observed peak powers

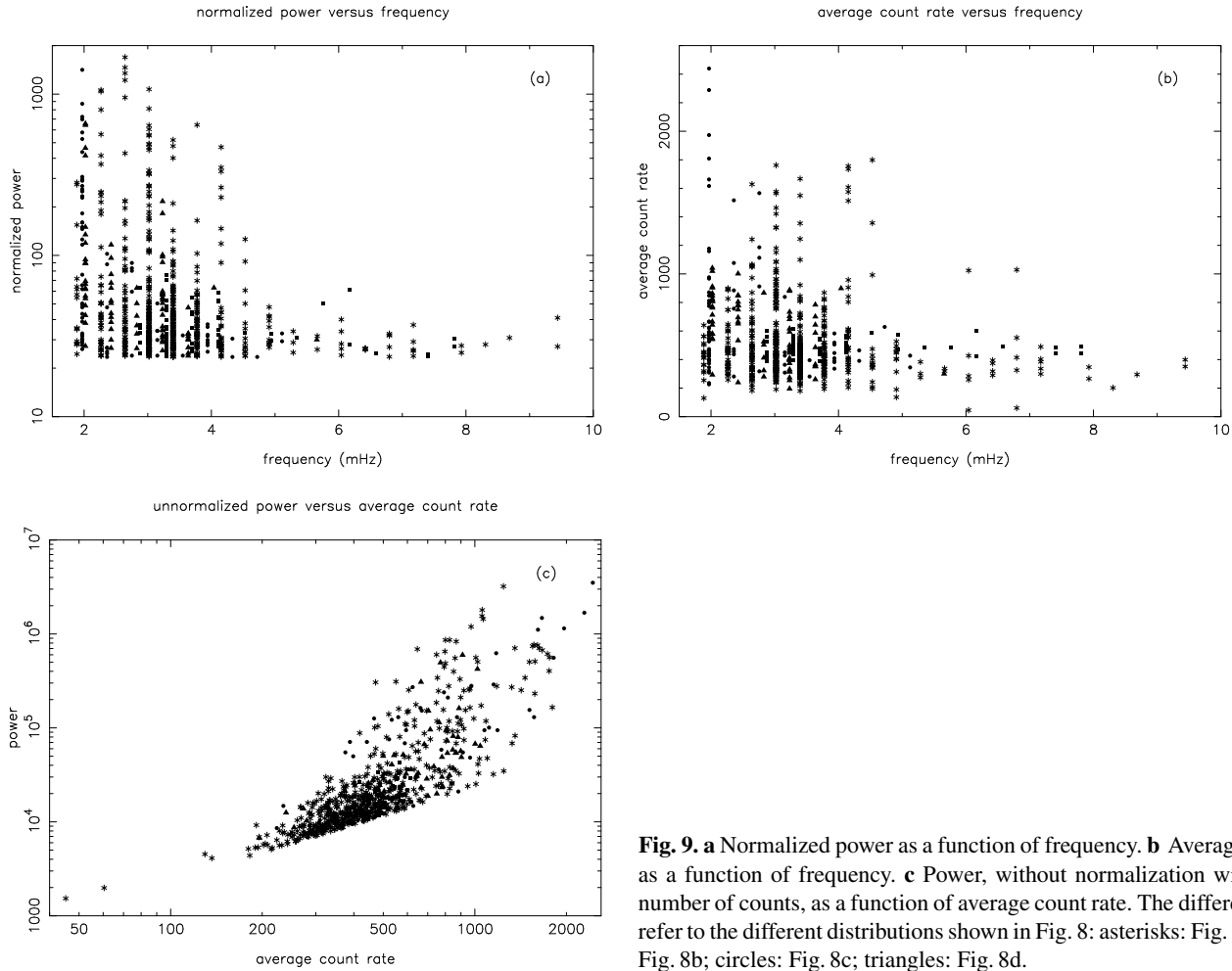


**Fig. 9.** **a** Normalized power as a function of frequency. **b** Average count rate as a function of counts, as a function of frequency. **c** Power, without normalization with the total number of counts, as a function of average count rate. The different symbols refer to the different distributions shown in Fig. 8: asterisks: Fig. 8a; squares: Fig. 8b; circles: Fig. 8c; triangles: Fig. 8d.

near 4.7 mHz as one would expect from the Carlsson and Stein simulations. On the contrary, the distribution is exactly located in the frequency range where the waves are *not* propagating. This strongly suggests that we are observing evanescent waves driven by the photospheric five minute oscillations.

The above explanation does not hold for the dataset showing an excessively large number of pixels with peak power at 2 mHz (Fig. 8c) because these are clearly related to flare-like variations. Porter et al. (1995) studied the correlation between (micro-)flares observed with the UVSP (C IV at 10<sup>5</sup> K) and the 3.5–5.5 keV emission as detected with the Hard X-ray Imaging Spectrometer (HXIS) on board the SMM. These authors find that small flare-like events detected in C IV have impulsive soft X-ray counterparts. It is possible that in our case (coronal) flare activity results in an increase of the emission measure at higher temperatures, say  $> 10^5$  K, so that the increase of the emission in the UVSP bandpass is related to optically thin emission from the transition region and the lower corona (see Fig. 2). This, and the origin of the 5 min. UVSP oscillations, can be tested by simultaneous observations of selected regions with the SUMER and CDS instruments onboard SOHO, thus covering spectral lines emitted from plasma temperatures ranging from 15,000 to 250,000 K.

It is, however, also possible that the high count rates are still flare-related but have their origin in the UV continuum formed near the temperature minimum. Orwig and Woodgate (1987) found a temporal correlation between hard X-ray bursts ( $> 30$  keV), ultraviolet line emission (O V at 1371 Å) and the UV continuum near 1600 Å. This led Machado and Mauas (1987) to propose a model in which irradiation by flare-related XUV emission (mainly C IV at 1549 Å) results in photo-ionization of Si I. This photo-ionization affects the continuum between 1350–1680 Å which is formed above the temperature minimum (Doyle and Phillips, 1992).

Both of the above presented explanations (TR/coronal emission or XUV irradiation) are based on coronal energy release and do not explain the 2 mHz (500 s.) periodicity. It is however simpler to relate a time scale of 500 s. to the corona than to the chromosphere. The 500 s. period could be related to the Alfvén bounce time in a short coronal loop, or to the periodicity of the sausage mode, so that a modulation of the energy release is present. The combination of 2 mHz oscillations and high count rates is only found in one of the datasets and is therefore a rather specific case.

The relative absence of significant power peaks above 5 mHz is striking. Of course there is power above 5 mHz in our power

spectra but apparently the bulk of the power is in evanescent waves. This can be explained if, apparently, evanescent waves oscillate more in phase, leading to a more (spatially) coherent oscillation and a 'clearer' modulation of the lightcurve. Above 5 mHz the waves are propagating and their phase relation is lost so that, in the field of view of a pixel, the compressions and rarefactions do not result in a strong modulation of the light curve.

Finally we note that our statistical treatment of the power spectra is very general and can equally be applied to SUMER and CDS data from SOHO.

*Acknowledgements.* Research at Armagh Observatory is grant-aided by the Dept. of Education for N. Ireland while partial support for software and hardware is provided by the STARLINK Project which is funded by the UK PPARC. EOS is supported via a studentship from Armagh Observatory. We are grateful to Drs. J. Gurman and S. Drake for their help in the reduction of the UVSP data and to Dr. J. Harvey for forwarding us the Kitt Peak data. This work was partly supported by PPARC grants GR/J30400 and GR/K43315. G.H.J. van den Oord acknowledges financial support from the Dutch Organization for Scientific Research (NWO).

## References

- Anders, E., Grevesse, N. 1989, *Geochimica and Cosmochimica Acta*, 53, 197
- Ando, H., Osaki, Y. 1975, *PASJ*, 27, 581
- Athay, R.G., White, O.R. 1979a, *ApJS*, 39, 333
- Athay, R.G., White, O.R. 1979b, *ApJ*, 229, 1147
- Bruner Jr., E.C. 1981, *ApJ*, 247, 317
- Bruner, M.E., Poletto, G. 1984, *Men. Soc. Astr. It.*, 55, 313
- Carlsson, M., Stein, R.F. 1992, *ApJ*, 397, L59
- Carlsson, M., Stein, R.F. 1994, in *Proceedings Mini-Workshop on Chromospheric Dynamics*, Ed. M. Carlsson, Inst. of Theor. Phys. Oslo, p. 47
- Carlsson, M., Stein, R.F. 1995, *ApJ*, 440, L29
- Carlsson, M., Stein, R.F. 1997, *ApJ*, 481, 500
- Chipman, E.G. 1978, *ApJ*, 224, 671
- Deubner, F.-L. 1981, in *The Sun as a star*, Ed. S. Jordan, NASA SP-450, p. 65
- Doyle, J.G., Phillips, K.J.H. 1992, *A&A* 257, 773
- Drake, S.A., Gurman, J.B. & L.E. Orwig, 1989, *Solar & stellar flares, IAU Coll 104, Catania Observatory Publication*, eds. B.M. Haisch & M. Rodono
- Gurman, J.B. Leibacher, J.W., Shine, R.A., Woodgate, B.E., Henze, W. 1981, in *The physics of sunspots*, p. 319
- Gurman, J.B. Leibacher, J.W., Shine, R.A., Woodgate, B.E., Henze, W. 1982, *ApJ*, 253, 939
- Henze, W., 1993, *Solar Maximum Mission/UVSP studies, Final Report SP93-NASA-3405*
- Henze, W., Tandberg-Hanssen, E., Reichmann, E.J., Athay, R.G. 1984, *Solar Phys.*, 91, 33
- Jenkins, G.M., Watts, D.G. 1968, *Spectral analysis and its applications*, Holden-Day, San Francisco
- Kaastra, J.S., Mewe, R., Nieuwenhuijzen, H. 1996, in *UV and X-ray spectroscopy of astrophysical and laboratory plasmas*, eds. K. Yamashita, T. Watanabe, Univ. Acad. Press, p. 411
- Leahy, D.A., Dabro, W., Elsner, R.F., Weisskopf, M.C., Sutherland, P.G., Grindlay, J.E. 1983, *ApJ*, 266, 160
- Lites, B.W., Chipman, E.G. 1979, *ApJ*, 231, 570
- Machado, M.E., Mauas, P.B. 1987, in *Rapid Fluctuations in Solar Flares*, NASA Conf. Publ. 2449, p. 271
- Narain, U., Ulmschneider, P., 1996, *Sp Sc Rev* 75, 453
- Orwig, L.E., Woodgate, B.E. 1987, in *Rapid Fluctuations in Solar Flares*, NASA Conf. Publ. 2449, p. 277
- Porter, J.G., Fontenla, J.M., Simnett, G.M. 1995, *ApJ*, 438, 472
- Rutten, R.J. 1995, in *Fourth SOHO Workshop Helioseismology*, ESA SP-376, p. 151
- Thomas J.H., Lites, B.W., Gurman, J.B., Ladd, E.F. 1987, *ApJ*, 312, 457
- van der Klis, M. 1989, in *Timing Neutron Stars*, eds. H. Ögelman, E.P.J. van der Heuvel, NATO ASI C262, Kluwer, Dordrecht, p. 27
- Vernazza, J.E., Avrett, E.H., Loeser, R. 1981, *ApJS*, 45, 635
- White, O.R., Athay, R.G. 1979a, *ApJS*, 39, 317
- White, O.R., Athay, R.G. 1979b, *ApJS*, 39, 347
- Woodgate et al., 1980, *Solar Phys.*, 65, 73